of our 40Gbit/s modulator driver, published in [2], were measured *on wafer* only. Since we found a similarly incorrect statement in two earlier publications, but by other authors and concerning our 60Gbit/s time-division multiplexer, we are concerned that such errors may propagate.

We therefore feel obliged to make the following statement: As pointed out in all of our Papers, we clearly prefer measurements on *mounted chips*. This is because we think that on-wafer measurements are only useful for preselection of the chips but not at all for the final characterisation of the circuit. The reason for this is that, in practice, only mounted chips can be used and that, therefore, the mounting parasitics have to be considered carefully in circuit design [3]. Thus it is our strict philosophy to present exclusively measurement results for mounted chips. This holds for *all* ICs in *all* work we have ever published.

H.-M. Rein, M. Möller and R. Schmid

Ruhr-University Bochum, AG Halbleiterbauelemente, D-44780 Bochum, Germany

References

1 THIAM, A., LEGROS, E., VUYE, S., ANDRÉ, P., WAWRZYNKOWSKI, E., and JOLY, C.: '40Gbit/s GaAs P-HEMT driver module for optical communications', *Electron. Lett.*, 1998, **34**, pp. 2232–2234

2 SCHMID, R., MEISTER, T.F., REST, M., and REIN, H.-M.: '40Gbit/s EAM driver IC in SiGe bipolar technology', *Electron. Lett.*, 1998, **34**, pp. 1095–1097

3 REIN, H.-M., and MÖLLER, M.: 'Design considerations for very-high-speed Si-bipolar ICs operating up to 50Gb/s', *IEEE J. Solid-State Circuits*, 1996, **31**, pp. 1076–1090

Electronics Letters Online No: 19990771
DOI: 10.1049/el:19990771

S. TEN BRINK: 'Convergence of iterative decoding', *Electron. Lett.*, 1999, **35**, (10), pp. 806–808

Editor's correction:

Convergence of iterative decoding

S. ten Brink

A novel method for visualising the convergence behaviour of iterative decoding schemes is proposed. Each constituent decoder is represented by a mutual information transfer characteristic which describes the flow of extrinsic information through the soft in/soft out decoder. The exchange of extrinsic information between constituent decoders is plotted in an extrinsic information transfer chart. The concepts are illustrated for an iterative demapping and decoding scheme.

Introduction: While many studies have concentrated on providing asymptotic bit error bounds for parallel and serially concatenated convolutional codes (e.g. [1]) little has yet been revealed as to the convergence behaviour of the corresponding sub-optimal iterative 'turbo' decoders. In this Letter a visualisation method based on bitwise mutual information is introduced which provides a tool for studying the convergence behaviour of iterative decoding schemes, yielding new design rules for improving the choice of constituent codes. For simplicity an iterative demapping and decoding scheme [2, 3] is considered in this Letter. The demapper takes soft values from the channel and outputs extrinsic information E_1 which is passed through a bit interleaver to become the *a priori* input A_2 for the soft in/soft out channel decoder [4]. From the decoder extrinsic information on the coded bits E_2 is fed back to the demapper as *a priori* knowledge A_1 to reduce the bit error rate (BER) in further iterative decoding steps. The variables A_1, E_1, A_2 and E_2 denote log-likelihood ratios (L-values).

Demapper transfer characteristics: The demapper transfer characteristic is a function of the *a priori* bitwise mutual information I_{A_1} and the E_b/N_0 value of the AWGN-channel

$$I_{E_1} = f(I_{A_1}, E_b/N_0) \qquad (1)$$

With equiprobable binary input symbols X to the mapper (at transmitter) the bitwise mutual information [5] is calculated as

$$I_{A_1} = \frac{1}{2}\sum_{x=0}^{1}\int_{-\infty}^{+\infty} p_{A_1}(\xi|X=x) \times \mathrm{ld}\frac{2p_{A_1}(\xi|X=x)}{p_{A_1}(\xi|X=0)+p_{A_1}(\xi|X=1)}d\xi \qquad (2)$$

For M bits per mapped codeword it is

$$I_{E_1} = \frac{1}{M}\sum_{k=0}^{M-1} I_{E_{1,k}} \qquad (3)$$

and

$$I_{E_{1,k}} = \frac{1}{2}\sum_{x=0}^{1}\int_{-\infty}^{+\infty} p_{E_1,k}(\xi|X=x) \times \mathrm{ld}\frac{2p_{E_1,k}(\xi|X=x)}{p_{E_1,k}(\xi|X=0)+p_{E_1,k}(\xi|X=1)}d\xi \qquad (4)$$

respectively. The conditional probability distributions p_{A_1} and $p_{E_{1,k}}$ for A_1 and $E_{1,k}$ are obtained by simulations. Different values of I_{A_1} and E_b/N_0 are considered in I_{E_1} through changes in the distributions $p_{E_{1,k}}$. Owing to the strong correlation between I_{A_1} and I_{E_1} the demapper characteristics can be plotted in an I_{E_1}, I_{A_1} diagram (Fig. 1), with the E_b/N_0 value as a parameter yielding a set of curves. Different distributions p_{A_1} were used to calculate the demapper characteristics without observing a notable change in the shape of the curves. Moreover, the demapper output distributions $p_{E_{1,k}}$ can be quite asymmetric and non-continuous with sharp edges, depending on the complex signal constellation and the applied mapping. Hence, transfer characteristics based on the mean values and variance of the input/output distributions, such as SNR measures, would fail, whereas mutual information transfer characteristics prove to be very robust, owing to the robustness of the entropy measure [5].

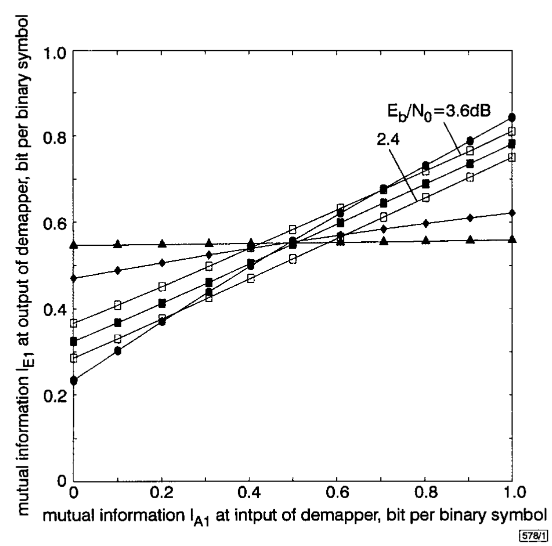

Fig. 1 *Extrinsic information transfer characteristics of 16-QAM demapper for different E_b/N_0 (at code rate 1:2) and different mappings*

—▲— Gray mapping (E_b/N_0 = 3dB)
—◆— some 16-QAM mapping (E_b/N_0 = 3dB)
—■— anti-Gray mapping (E_b/N_0 = 3dB)
—●— some 16-QAM mapping (E_b/N_0 = 3dB)
—□— anti-Gray mapping, different E_b/N_0 values

The demapper transfer characteristics almost approach straight lines. Thus it is sufficient to describe a mapping using two values: the bitwise mutual information $I_0 = I_{E_1}(I_{A_1} = 0)$ given that no other bit of the mapping is known ('no *a priori* knowledge at demapper'), and $I_{all} = I_{E_1}(I_{A_1} = 1)$ given that all other bits of the mapped codeword are known ('perfect *a priori* knowledge') [2]. Keeping the mapping fixed, different E_b/N_0 values just shift the curve up and down. Keeping the E_b/N_0 value fixed, different mappings result in lines of different slope. For Gray mapping the bitwise mutual information remains almost constant with increasing *a priori* knowledge I_{A1}, whereas the transfer characteristic for anti-Gray mapping has a steep slope, revealing the strong potential performance improvements in an iterative demapping and decoding scheme.

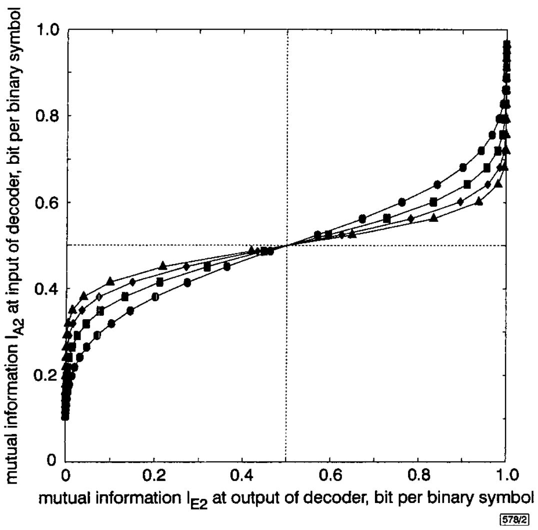

Fig. 2 *Extrinsic information transfer characteristics of soft in/soft out decoder for rate 1:2 convolutional codes with different memory*

—●— rate 1:2, memory 2
—■— rate 1:2, memory 4
—◆— rate 1:2, memory 6
—▲— rate 1:2, memory 8

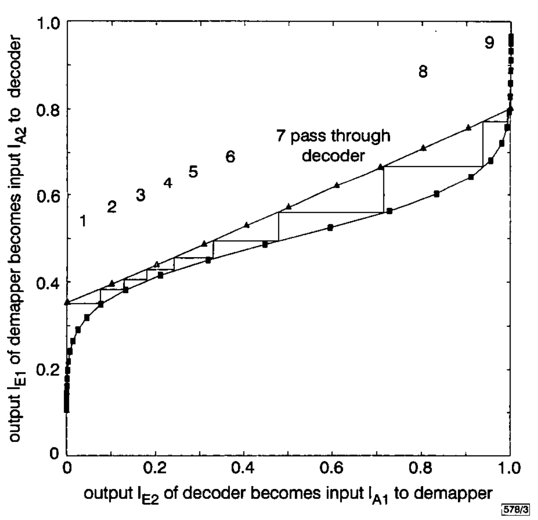

Fig. 3 *Example of trajectory for iterative decoding at E_b/N_0 = 3.4dB, 16-QAM, anti-Gray mapping, rate 1:2 memory 4 code*

——— trajectory of iterative decoding
—▲— anti-Gray mapping (E_b/N_0 = 3.4dB)
—■— conv. code, rate 1:2, memory 4

Decoder transfer characteristics: Corresponding to eqns. 2 – 4 the decoder transfer characteristic on the coded bits is defined as

$$I_{E_2} = g(I_{A_2}) \qquad (5)$$

It is only dependent on the bitwise mutual information I_{A_2} of the *a priori* input to the decoder. Again, the probability distributions p_{E_2}, p_{A_2} for calculating I_{E_2}, I_{A_2} are obtained by simulation.

Fig. 2 shows the transfer characteristics for convolutional codes of rate 1:2 with memory 2, 4, 6 and 8. It is remarkable that all curves cross at a single point: (0.5, 0.5). For arbitrary code rates R this point turns out to be at (0.5, R).

Extrinsic information transfer chart: Connected through interleavers, the extrinsic output of the demapper becomes the *a priori* input to the decoder $I_{A_2} = I_{E_1}$, and the extrinsic output of the decoder becomes the *a priori* input to the demapper $I_{A_1} = I_{E_2}$. This exchange of extrinsic information is accounted for in the extrinsic information transfer chart (EIT chart) by plotting the demapper and decoder characteristics into a single diagram.

Fig. 3 shows an example of an iterative decoding trajectory: the E_b/N_0 value of the channel has raised the demapper curve just high enough to open a tunnel for the trajectory. This matches with the BER(E_b/N_0) plot of [2] where the turbo cliff is at ~3.3dB. The BER floor is determined by the intersection of demapper and decoder curves on the very right side of the EIT chart. Note that mutual information (decoder output on the information bits, not shown) and BER are connected through a bound given by the converse of the coding theorem [5]. Both demapper and decoder characteristics are obtained *separately*, and not in conjunction with a particular iterative decoding scheme; for verification, the trajectory of Fig. 3 has been evaluated by means of simulation. Clearly, the trajectory closely matches the demapper and decoder characteristics. For short interleavers the trajectory would tend to diverge from the characteristics after a few iterations. From the EIT chart some design guidelines become apparent, for example, the larger the code memory, or the steeper the slope of the demapper curve, the later the turbo cliff in the BER(E_b/N_0) chart, but the lower the BER floor.

Conclusions: It has been shown that the transfer characteristics based on mutual information can facilitate the design of iterative demapping schemes. The flow of extrinsic information was visualised in the EIT chart to provide insight into the turbo cliff position and BER floor. Initial results for other concatenated codes [1, 6] are encouraging.

Acknowledgment: This work was carried out in a joint project with Bell Laboratories, Lucent Technologies, Pagoda Park, Swindon, Wiltshire SN5 7YT, United Kingdom.

22 February 1999
Electronics Letters Online No: 19990555
DOI: 10.1049/el:19990555

S. ten Brink (*University of Stuttgart, Room 2.333, Institute of Telecommunications, Dep. 0408, Pfaffenwaldring 47, 70569 Stuttgart, Germany*)

E-mail: tenbrink@inue.uni-stuttgart.de

References

1 BENEDETTO, S., DIVSALAR, D., MONTORSI, G., and POLLARA, F.: 'Serial concatenation of interleaved codes: performance analysis, design, and iterative decoding', *IEEE Trans.*, 1998, **IT-44**, (3), pp. 909–926

2 TEN BRINK, S., SPEIDEL, J., and YAN, R.-H.: 'Iterative demapping and decoding for multilevel modulation'. Proc. IEEE GLOBECOM'98, Sydney, Australia, 1998, pp. 579–584

3 TEN BRINK, S., SPEIDEL, J., and YAN, R.-H.: 'Iterative demapping for QPSK modulation', *Electron. Lett.*, 1998, **34**, (15), pp. 1459–1460

4 ROBERTSON, P., VILLEBRUN, E., and HOEHER, P.: 'A comparison of optimal and sub-optimal MAP decoding algorithms operating in the log domain'. Proc. ICC '95, June 1995, pp. 1009–1013

5 HAMMING, R.W.: 'Coding and information theory' (Prentice-Hall, New Jersey, 1986)

6 BERROU, C., GLAVIEUX, A., and THITIMAJSHIMA, P.: 'Near Shannon limit error-correcting coding and decoding: Turbo-codes'. Proc. ICC'93, May 1993, pp. 1064–1070

BOUTTOUT, F., BENABDELAZIZ, F., BENGHALIA, A., KHEDROUCHE, D., and FORTAKI, T.: 'Uniaxially anisotropic substrate effects on resonance of rectangular microstrip patch antenna, *Electron. Lett.*, 1999, **35**, (4), pp. 255–256

Editor's correction:

In the caption of Fig. 2, the permittivities for the positive uniaxial case should read $\varepsilon_x = 5$, $\varepsilon_z = 6.4$

Author's correction:

On p. 256, the second line of the paragraph below Fig. 3, 'Figs. 1 and 2,' should read 'Figs. 2 and 3'.

YOUNSEOK CHOO: 'Improvement to modified Routh approximation method', *Electron. Lett.*, 1999, **35**, (7), pp. 606–607

Author's correction:

The third line of eqn. 1 should have appeared as below:

$$\frac{M_1}{s} + \frac{M_2}{s^2} + \frac{M_3}{s^3} + \cdots$$

LAMBOTHARAN, S., CHAMBERS, J.A., and CONSTANTINIDES, A.G.: 'Adaptive blind retrieval techniques for multiuser DS-CDMA signals' *Electron. Lett.*, 1999, **35**, (9), pp. 693–695

Editor's correction:

Reference [8] should read:

8 LAMBOTHARAN, S., and CHAMBERS, J.A.: On the surface characteristics of a mixed constant modulus and cross-correlation criterion for the blind equalization of a MIMO channel', *Signal Process.*, 1999, **74**, pp. 209–216

LEVITA, C.J.A., WASSELL, I.J., and BENAISSA, M.: 'Coded and uncoded CPM schemes over rings of integers for AWGN and Rayleigh fading channels', *Electron. Lett.*, 1999, **35**, (9), pp. 696–698

Editor's correction:

Fig. 2 should have appeared as below:

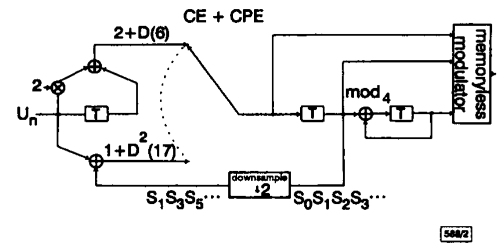

ESTIMATION OF LENGTH FOR *ELECTRONICS LETTERS* VERSION 5.1

As set by our typesetters, the maximum length in print of a Letter is 83 column cms, or three columns of about 27cms height. When judging the length of a submission, please take into account:

Title 0.5 column cm per 40 characters (or part thereof)

Abstract 1 column cm per 165 characters

Authors 1 column cm per separate affiliation

Text 1 column cm per 165 characters (it is easiest to estimate the number of characters, including spaces, per line and the number of lines per page)

References 1 column cm each

Tables 0.4 column cm per line

Figures All figures are reduced to a width of 8.6cm. If the figure is wider than it is high, divide the height by the width and multiply by 8.6 column cm. If the figure is higher than it is wide (discouraged), the figure will occupy more than 8.6 column cm.

Captions 1 column cm per main figure or table caption (provided it is brief), 0.33 column cm per line for subcaptions (including keys and other information that will be removed from the figures).

Equations

Single line equations:	0.6–0.8	column cm per line
Integrals:	1.0	column cm per line
Quotients:	0.7–1.2	column cm per line
Sums and products:	1.2	column cm per line
Matrices:	0.4	column cm per line

For other equation types, refer to a recent issue of *Electronics Letters*. Excessively long equations will be split into several lines.